THE ASTRONOMICAL JOURNAL, 120:1106–1112, 2000 August

INTERFEROMETRIC ASTROMETRY OF THE LOW-MASS BINARY Gl 791.2 (=HU DEL) USING *HUBBLE SPACE TELESCOPE* FINE GUIDANCE SENSOR 3: PARALLAX AND COMPONENT MASSES[1]

G. FRITZ BENEDICT,[2] BARBARA E. MCARTHUR,[2] OTTO G. FRANZ,[3] LAWRENCE H. WASSERMAN,[3] AND TODD J. HENRY[4]

Received 1999 October 5; accepted 2000 March 26

ABSTRACT

With fourteen epochs of fringe-tracking data spanning 1.7 yr from Fine Guidance Sensor 3 we have obtained a parallax ($\pi_{abs} = 113.1 \pm 0.3$ mas) and perturbation orbit for Gl 791.2A. Contemporaneous fringe-scanning observations yield only three clear detections of the secondary on both interferometer axes. They provide a mean component magnitude difference, $\Delta V = 3.27 \pm 0.10$. The period ($P = 1.4731$ yr), from the perturbation orbit, and the semimajor axis ($a = 0.963 \pm 0.007$ AU), from the measured component separations with our parallax, provide a total system mass $M_A + M_B = 0.412 \pm 0.009\ M_\odot$. Component masses are $M_A = 0.286 \pm 0.006\ M_\odot$ and $M_B = 0.126 \pm 0.003\ M_\odot$. Gl 791.2A and Gl 791.2B are placed in a sparsely populated region of the lower main-sequence mass-luminosity relation where they help *define* the relation because the masses have been determined to high accuracy, with errors of only 2%.

Key words: astrometry — binaries: general — stars: distances — stars: individual (Gliese 791.2) — stars: late-type — stars: low-mass, brown dwarfs

1. INTRODUCTION

The dependence of intrinsic brightness upon mass, the mass-luminosity relation (MLR), is fundamental to our understanding of stellar astronomy. The MLR is relevant to studies of the evolution of individual stars and is required to convert a luminosity function into a mass function for determinations of the mass content of the Galaxy. The MLR can also be folded into efforts to determine the ages of stellar clusters. In addition, at masses less than 0.1 $M_\odot$ the MLR is critical for brown dwarf studies, because mass remains an important determinant in culling brown dwarfs from stars. Despite its broad utility, the MLR remains poorly determined for M dwarfs, by far the dominant population of the Galaxy in both numbers (>70%) and stellar mass contribution (>40%; Henry 1998). To improve the low-mass MLR, we are observing nearby red dwarf multiple systems to determine masses accurate to 5% or better.

Gl 791.2 (HU Del = LHS 3556, R.A. = $20^h29^m48^s.0$, decl. = $+09°41'23''$, epoch and equinox 2000.0) is an example of an M dwarf binary with at least one component in the 20-20-20 Sample, which was defined by Henry et al. (1999) to include systems having $d \leq 20$ pc, $M \leq 0.20\ M_\odot$, and orbital period $P \leq 20$ yr. Gl 791.2 was discovered to be binary by Harrington (1971), who determined a semimajor axis for the photocentric orbit of 0".029, with a period of 1.5 yr, and estimated the companion mass to be 0.07–0.11 $M_\odot$. The perturbation was confirmed by Hershey (1978), who found nearly identical values for the semimajor axis, period, and mass estimate, and suggested that "Such a pair may be resolvable with a space telescope. One reliable observation of separation and magnitude would yield good masses for both members."

Using infrared speckle techniques, McCarthy (1986) attempted to resolve the pair but was unsuccessful. Continued attempts by one of us (Henry) using infrared speckle imaging detected the companion [$\Delta H(1.6\mu m) \leq 1.3$] but did not result in clear resolution because of the close separation (maximum ~0".15). The observation did indicate that the magnitude difference was not extreme (presumably even at optical wavelengths), so that the system might be resolved with Fine Guidance Sensor 3 (FGS 3) on the *Hubble Space Telescope* (*HST*). Most importantly, FGS 3 offered resolution capability to 20 mas, about 10 times better than the infrared speckle observations. With the suspicion that the secondary is an important object with a mass near 0.1 $M_\odot$ in a small but resolvable orbit, we obtained 14 usable fringe-tracking observation sets with *HST* to obtain the precise parallax and component masses reported in this paper.

Table 1 provides aliases and physical parameters for the Gl 791.2 system. The radius is predicted from the model of Burrows et al. (1993) and is comparable to the radii of the red dwarf components of CM Draconis, 0.25 and 0.23 $R_\odot$, determined by Metcalfe et al. (1996), which have masses of 0.23 and 0.21 $M_\odot$, respectively. Finally, Delfosse et al. 1998 find Gl 791.2 to be a rapid rotator and from space velocities assign it to the young disk population.

2. DATA REDUCTION AND CALIBRATION PROCEDURES

Our observations were obtained with FGS 3, a two-axis, white-light interferometer aboard *HST*. This instrument has two operating modes; fringe tracking (POS) and fringe scanning (TRANS). We time-tagged our data with a Modified Julian Date, MJD = JD − 2,400,000.5. We obtained a total of 15 observation sets. Unfortunately the POS observations at MJD 50,534.04 suffered from over 50 mas of drift. Satisfactory correction was unobtainable, so we discarded these data. Table 2 presents a log of the successful POS

[1] Based on observations made with the NASA/ESA *Hubble Space Telescope*, obtained at the Space Telescope Science Institute, which is operated by the Association of Universities for Research in Astronomy, Inc., under NASA contract NAS5-26555.

[2] McDonald Observatory, University of Texas at Austin, TX 78712-1083.

[3] Lowell Observatory, 1400 West Mars Hill Road, Flagstaff, AZ 86001.

[4] Department of Physics and Astronomy, Johns Hopkins University, 3400 North Charles Street, Baltimore, MD 21218.

TABLE 1

GL 791.2 = G 24−16 = LHS 3556 = HU DEL

Parameter	Value	Reference
V	13.06 ± 0.03	Leggett 1992
$B-V$	1.66 ± 0.05	Leggett 1992
Spectral Type	M4.5 V	Kirkpatrick, Henry, & McCarthy 1991
R_A	$0.18\ R_\odot$	Burrows et al. 1993
V_A(rot)	32 ± 2 km s^{-1}	Delfosse et al. 1998

observations used in this investigation. Note that each observation set contains either two or three observations of the primary science target, Gl 791.2, because a single long visit has been split into shorter, independent measurements.

TABLE 2

POS OBSERVATIONS OF GL 791.2A AND PERTURBATION ORBIT RESIDUALS

Obs. Set	MJD	ρ_A (mas)	θ (deg)	$\Delta\rho_A$ (mas)	$\Delta\theta$ (deg)	$\rho_A\Delta\theta$ (mas)
1	49,950.1779	16.0	95.1	0.3	5.6	1.6
1	49,950.1952	15.9	95.1	0.4	5.0	1.4
2	49,970.9509	16.1	139.8	0.4	−2.3	−0.7
2	49,970.9682	16.1	139.8	0.4	−5.1	−1.4
3	49,997.8257	21.4	183.6	−0.9	−8.0	−3.0
3	49,997.8430	20.9	183.6	−0.4	−7.1	−2.6
4	50,025.5061	26.8	208.6	0.0	1.5	0.7
4	50,025.5234	27.3	208.6	−0.6	0.0	0.0
5	50,050.6372	32.4	222.5	0.0	5.3	3.0
5	50,050.6545	32.7	222.5	−0.3	5.0	2.8
6	50,167.3154	48.0	256.1	−0.5	2.1	1.8
6	50,167.3327	49.8	256.1	−2.3	3.0	2.6
7	50,194.5250	48.8	261.8	−0.6	1.9	1.6
7	50,194.5423	47.7	261.8	0.5	0.9	0.8
8	50,236.9474	47.0	270.7	0.5	−1.0	−0.8
8	50,236.9647	47.3	270.7	0.2	−0.2	−0.2
9	50,255.2418	49.5	274.7	−3.0	−1.6	−1.4
9	50,255.2591	49.7	274.7	−3.3	−1.1	−1.0
10	50,338.7445	38.2	297.1	−1.4	−1.7	−1.2
10	50,338.7618	37.5	297.1	−0.7	2.3	1.5
10	50,338.7684	38.6	297.1	−1.8	−1.3	−0.9
11	50,372.9877	33.6	311.3	−2.8	3.4	2.0
11	50,373.0050	33.4	311.3	−2.6	3.6	2.1
11	50,373.0117	32.7	311.3	−2.0	5.2	3.0
12	50,398.5885	25.9	326.5	−0.1	8.4	3.8
12	50,398.6058	26.3	326.5	−0.5	8.0	3.7
12	50,398.6125	27.0	326.5	−1.1	7.9	3.7
13	50,424.6554	21.2	349.5	0.1	5.6	2.1
13	50,424.6727	22.1	349.5	−0.8	5.9	2.3
13	50,424.6793	23.0	349.5	−1.7	3.4	1.4
14	50,569.0266	28.3	212.1	−0.5	−2.2	−1.1
14	50,569.0439	29.1	212.1	−1.3	−3.3	−1.7
14	50,569.0505	29.7	212.1	−1.9	−3.8	−2.0
$\langle \lvert \text{res} \rvert \rangle$[a]				1.0	3.7	1.8

[a] For $N = 33$.

Table 3 presents a log of those TRANS observations that yielded total component separations, position angles, and magnitude differences. These TRANS data are discussed in § 2.3.

Bradley et al. (1991) provide an overview of the FGS 3 instrument. Our goal, precision small-field astrometry with 1 mas per observation, has been achieved, but not without significant challenges. These included a mechanically noisy on-orbit environment, the self-calibration of FGS 3, and significant temporal changes in our instrument. Benedict et al. (1998, 1999) review our solutions to these problems, including a denser set of drift-check stars for each science observation, fine-tuning exposure times, overlapping field observations and analyses for calibration, and a continuing series of trend-monitoring observations. McArthur et al. (1999) and Benedict et al. (1999) describe data acquisition and reduction strategies for derivation of parallax and proper motion.

The present investigation poses the added complexity of reflex motion of the target due to a faint companion. Hence our GAUSSFIT (Jefferys, Fitzpatrick, & McArthur 1988) model was modified to allow for the simultaneous estimation of the astrometric parameters (ξ and η), parallax (π), and proper motion (μ_x and μ_y), as well as the seven standard orbital parameters (see Table 6). We first place all the reference-star measurements into a common reference frame by determining scale, orientation, and offset parameters for each observation set. These are "plate" constants. We then apply these to the Gl 791.2A measurements to obtain the parallax, proper motion, and orbital elements.

2.1. *Gl 791.2 Astrometric Reference Frame*

Table 4 lists the three stars in the Gl 791.2 reference frame. Figure 1 shows the distribution in FGS 3 instrumental coordinates of the 14 sets of reference-star measurements used to establish the reference frame. The circular pattern is impressed by the requirement that *HST* roll to keep its solar panels fully illuminated throughout the year. From these data we determine the scale, rotation, and offset "plate constants" relative to an arbitrarily adopted constraint epoch (the so-called master plate) for each observation set. With a sufficient number of reference stars we normally obtain six plate constants per observation set,

TABLE 3

TRANS OBSERVATIONS OF GL 791.2B AND RESIDUALS

Set	MJD	ρ_A (mas)	θ (deg)	$\Delta\rho_A$ (mas)	$\Delta\theta$ (deg)	$\rho_A\Delta\theta$ (mas)	Δm_X^c	Δm_Y
8	50,235.94744	169.2	89.2	7.4	0.0	0.0	3.40	3.12
9	50,254.24177	153.3	84.6	−5.2	−0.7	−1.8	3.54	3.43
10	50,337.74448	126.0	62.9	−0.3	0.3	0.2	3.14	3.30
$\langle \lvert \text{res} \rvert \rangle$[a]				4.3	0.3	0.7	3.36	3.28

[a] For $N = 3$.

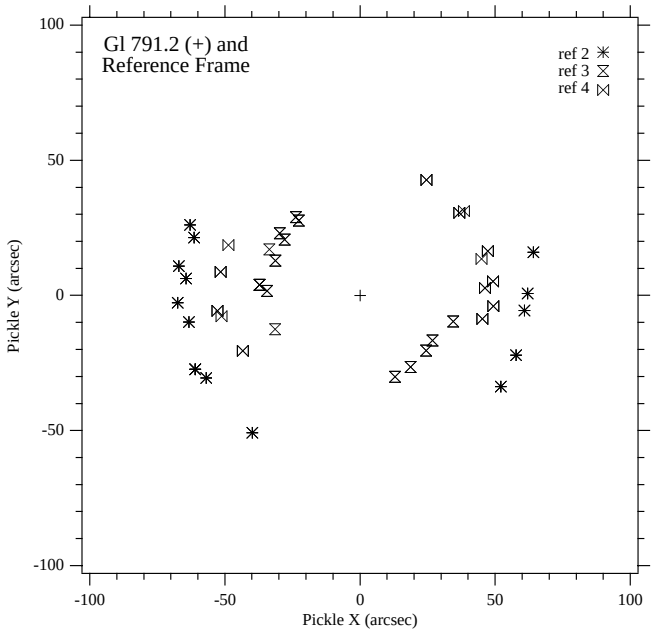

FIG. 1.—Gl 791.2 and reference-frame observations in FGS 3 pickle coordinates. Symbols identify each star listed in Table 3.

allowing the scale in X to differ from the scale in Y. We also determine the parallax and proper motion of each reference star. The Gl 791.2 reference frame contains only three stars. Hence, we constrained the scales along the X and Y axes to equality and the two axes to orthogonality. We also constrained the proper motions and parallaxes to have values of zero. The model becomes

$$\xi = aX + bY + c\,, \tag{1}$$

$$\eta = -bX + aY + f\,, \tag{2}$$

where a, b, c, and f are the plate constants, relating each observation set to the master plate. The orientation with respect to the sky of the observation set chosen to be the constraint epoch is determined with star positions from the USNO-A2.0 catalog (Monet 1998) with uncertainties in the field orientation of $\pm 0\overset{\circ}{.}03$.

The final reference-frame model produces plate constants from the 91 reference-star observations contained in the 14 observation sets. (Each set contains one to three observations of each reference star.) It also produces residuals for each reference star. From the histograms of the X and Y residuals (Fig. 2) we conclude that we have obtained plate constants that map each observation set to the others at the 1 mas level. To determine whether there might be unmodeled but eventually correctable systematic effects, we plotted

TABLE 4

GL 791.2 REFERENCE-FRAME RELATIVE POSITIONS

Star	V	$B-V$	ξ (arcsec)	η (arcsec)
Ref 2	12.1	1.9	$109\overset{''}{.}8430 \pm 0\overset{''}{.}0009$	$29\overset{''}{.}0122 \pm 0\overset{''}{.}0011$
Ref 3	14.8	1.5	$78\overset{''}{.}4308 \pm 0.0010$	$5\overset{''}{.}4658 \pm 0.0011$
Ref 4[a].....	14.8	1.6	$0\overset{''}{.}0000 \pm 0.0017$	$0\overset{''}{.}0000 \pm 0.0023$

[a] R.A. = $307\overset{\circ}{.}43704$, decl. = $9\overset{\circ}{.}68324$, J2000.0, epoch 1995.843.

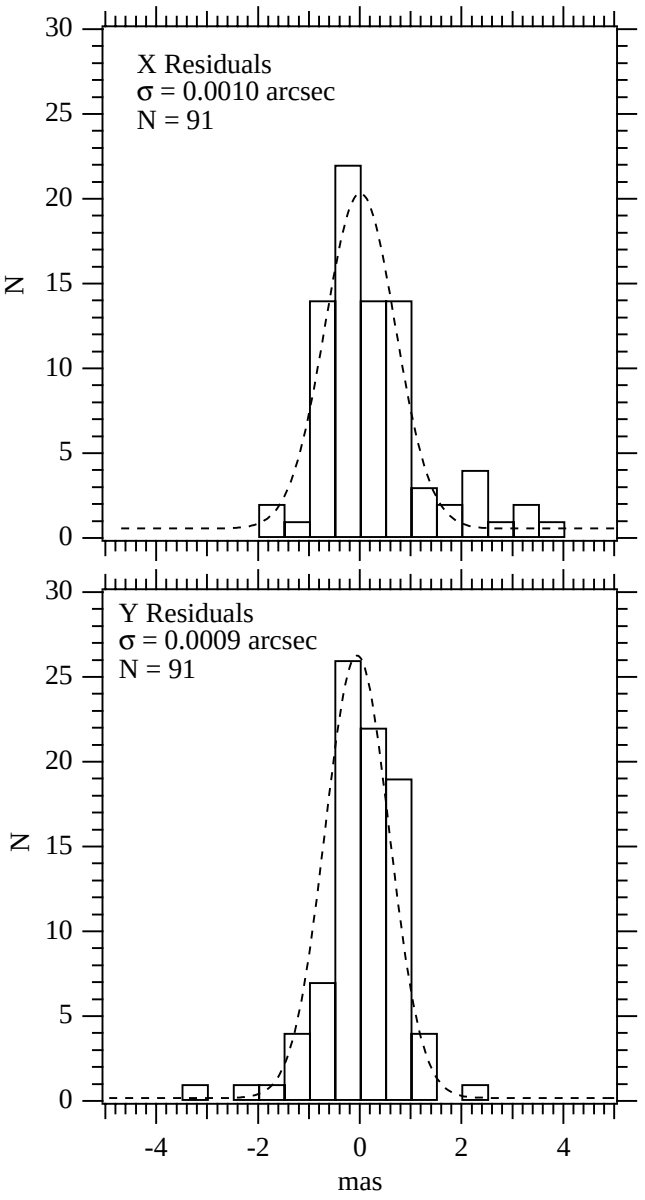

FIG. 2.—Histograms of X and Y residuals obtained from modeling the Gl 791.2 reference frame with equations (1) and (2). Distributions are fitted with Gaussians.

the Gl 791.2 reference-frame X and Y residuals against a number of spacecraft, instrumental, and astronomical parameters. These included X and Y position within the FGS 3 field of regard (the so-called pickle), radial distance from the pickle center, reference-star V magnitude and $B-V$ color, and epoch of observation. No trends were seen above the 1.0 mas level. The resulting catalog of positions for the three reference stars is given in Table 4, where ξ and η are parallel to right ascension and declination, respectively.

2.2. *Modeling the Parallax, Proper Motion, and Orbital Motion of Gl 791.2A*

Once we have determined plate constants by applying equations (1) and (2) to the reference frames, we apply the transformations to the Gl 791.2A fringe-tracking measurements (FGS POS mode) and solve for parameters describ-

ing relative parallax, proper motion, and orbital motion, modifying the equations appropriately:

$$\xi = aX + bY + c - P_x * \pi - \mu_x * t - \mathrm{ORBIT}_x , \quad (3)$$

$$\eta = -bX + aY + f - P_y * \pi - \mu_y * t - \mathrm{ORBIT}_y , \quad (4)$$

where a, b, c, and f are the plate constants obtained from the reference frame, P_x and P_y are the parallax factors, and t is the time of observation. We obtain the parallax factors, P_x and P_y, from a Jet Propulsion Laboratory Earth orbit predictor (DE200; Standish 1990). ORBIT is a function of the traditional orbital elements, listed in Table 6.

From the photometry in Tables 1 and 4, we see that the colors of the reference stars and the target are all red. Therefore, we apply no corrections for lateral color (Benedict et al. 1999). Reference-frame colors were obtained from the USNO-A2.0 catalog (Monet 1998). Calibration from the catalog $b-r$ colors to $B-V$ was obtained from the Barnard's star and lateral color calibration field photometry in Benedict et al. (1999). We obtained a zero-point correction from the Leggett (1992) photometry of Gl 791.2.

Given the uncorrected *HST* point-spread function (PSF) for the FGSs (they are not in the COSTAR path), we must discuss photocenter corrections (e.g., van de Kamp 1967). The FGS transforms the images of the two components into two fringes. As long as the components are more widely separated than the resolution of *HST* at $\lambda = 580$ nm, about 40 mas, the presence of a companion has no effect on the centroid obtained from the fringe-zero crossing. However, what matters is the separation along each interferometer axis, not the total separation on the sky. For any arbitrary orientation, components A and B can have separations along the FGS axes from 0.0 mas to the actual full separation. For example observation set 6 in Table 2 the total separation along the X axis is 151 mas, but only 26 mas along Y.

Simulations were done to characterize the effect the secondary has on the position derived for the primary for separations less than 40 mas. First, we obtained a position derived from a fringe scan of a single star of appropriate color. Then, a companion with $\Delta V = 3.25$ was placed at separations of ± 5, ± 10, ± 20, ± 35, ± 50, and ± 100 mas along each axis. As can be seen in Franz et al. (1998; Fig. 1), the interferometer response functions are not symmetric about the zero crossing. Hence the simulation required that the companion be placed on either side of the primary. Fitting each synthetic binary TRANS scan as a single star will quantify the effect of the undetected companion on the measured position of the primary. In no case did the position of the primary move from the single-star location by more than 0.6 mas, less than the error in the measurement of its position.

Every small-field astrometric technique requires a correction from relative to absolute parallax because the reference-frame stars have an intrinsic parallax. We adopt the methodology discussed in the Yale Parallax Catalog (van Altena, Lee, & Hoffleit 1995, § 3.2, Fig. 2, hereafter YPC95). From Figure 2 in YPC95, the Gl 791.2 galactic latitude, $b = -16\overset{\circ}{.}8$, and average magnitude for the reference frame, $\langle V_{\mathrm{ref}} \rangle = 13.9$, we obtain a correction to absolute of 1.0 ± 0.2 mas. Applying this correction results in the absolute parallax of 112.9 ± 0.3 mas listed in Table 5. This compares favorably with the YPC95 parallax, 113.8 ± 1.9 mas, and represents a sixfold reduction in the error. With

TABLE 5

Gl 791.2 Parallax and Proper Motion

Parameter	Value
HST study duration	1.7 yr
Number of observation sets	14
Reference stars $\langle V \rangle$	13.9 ± 1.6
Reference stars $\langle B-V \rangle$	1.7 ± 0.2
HST relative parallax	111.9 ± 0.2 mas
Correction to absolute	1.0 ± 0.2 mas
HST absolute parallax	112.9 ± 0.3 mas
HST proper motion	678.8 ± 0.4 mas yr^{-1}
In position angle	$79\overset{\circ}{.}62 \pm 0\overset{\circ}{.}03$
Yale Parallax Catalog 1995	113.8 ± 1.9 mas
Proper motion[a]	678.6 mas yr^{-1}
In position angle	$79\overset{\circ}{.}0$

[a] Harrington & Dahn 1980.

$V = 13.06$, Gl 791.2 is too faint to have been observed by *Hipparcos*.

The final absolute parallax formal uncertainty includes the estimated error in the correction to absolute, added in quadrature to the relative parallax error. Our confidence in the correction to absolute (± 0.2 mas) comes from comparisons carried out by Harrison et al. (1999) and Benedict et al. (1999). They compared corrections with absolute parallaxes derived from spectroscopy of reference-frame stars with the correction obtained from YPC95. Differences averaged around 0.2 mas.

2.3. *Orbit from Fringe-Tracking and Scanning Observations*

If the secondary in a binary system can be detected directly, both the magnitude difference between the components (needed to measure the luminosity for the MLR) and their total separation (needed to measure the mass for the MLR) can be determined. We detect only component A of Gl 791.2 in the POS measurements, but Gl 791.2B was detected at three epochs using FGS 3 TRANS measurements. These data are acquired at the midpoint of each observation set (orbit) listed in the observation log (Table 2). Details of the fringe-scanning analysis procedure are presented in Franz et al (1998).

The observed fringe is treated as a linear superposition of two single-star fringes. Two single-star fringe templates are fitted to the observed binary system fringe pattern, minimizing the residuals in a least-squares sense, with ΔF583W (F583W is the name of the filter used) and component separation as free parameters on each axis. The X and Y axes are fitted independently because there are, in fact, two interferometers within each FGS. Fringe-scanning observations were obtained during each of the 14 observation sets listed in Table 2. The template used for deconvolution of both sources was from a single star with $B-V = 1.9$, similar to both components of Gl 791.2.

We obtained only three pairs of detections of the secondary in 30 attempts (counting each axis as a separate attempt), indicating that component B is a challenging target for FGS 3. All of these detections were near maximum elongation, and the companion was clearly seen on both axes. Measuring the full separation and position angle requires resolution along both the X and Y axes at each epoch. At two other epochs near maximum elongation (sets 6 and 7, Table 2) a separation was measured, but it required that we constrain the magnitude difference on one

TABLE 6

GL 791.2AB ORBIT

Parameter	Value
a	108.8 ± 0.7 mas
α_A	33.2 ± 0.2 mas
α_B	75.6 ± 0.7 mas
f	0.3051 ± 0.0031
a	0.963 ± 0.007 AU
P	1.4731 ± 0.0008 Y
T	1998.5668 ± 0.0013
e	0.519 ± 0.003
i	$145\overset{\circ}{.}7 \pm 0\overset{\circ}{.}7$
Ω'	$104\overset{\circ}{.}5 \pm 0\overset{\circ}{.}2$
Ω	$-75\overset{\circ}{.}5 \pm 0\overset{\circ}{.}2$
ω'	$12\overset{\circ}{.}8 \pm 0\overset{\circ}{.}3$

axis. This was due to the projected separation along that axis being less than 25 mas. Because constraining ΔF583W does not yield an independent detection in these cases, we have removed these epochs from further consideration.

The successful two-axis detections are detailed in Table 3 and plotted with the component A perturbation orbit in Figure 4. We note that the X and Y positions used to derive the fringe-scanning separations (in Table 3, ρ for the total separation) have been corrected for the instrumental effect discussed in Franz et al. (1998, § 4.1).

Our orbital parameters for components A and B are presented in Table 6. All parameters describing this orbit are derived from all the component A POS measurements (Table 2) and the three independent TRANS observations (Table 3) in a simultaneous solution. Primed parameters refer to the perturbation orbit. In Figure 3 we show the residual vectors for each of the two or three POS mode observations at each epoch. Listed in Table 2, the residuals to the perturbation orbit range from 0 to 5 mas with an

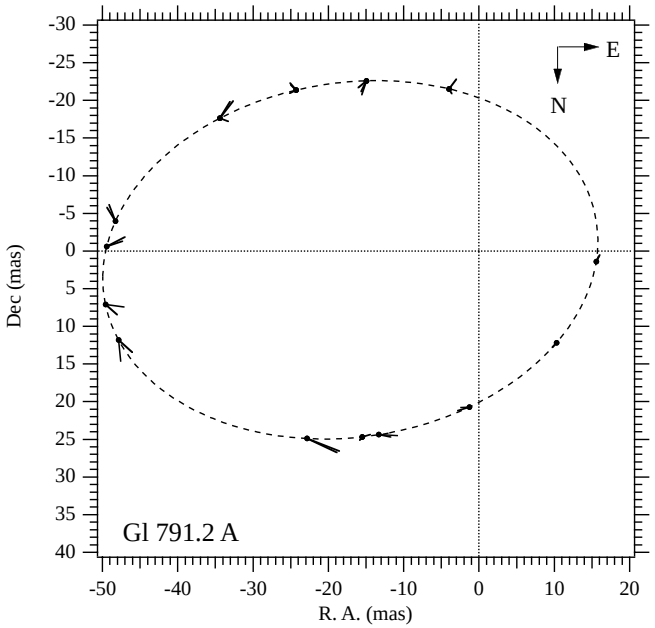

FIG. 3.—Perturbation orbit for Gl 791.2A, showing predicted positions at each epoch of observation (*circles*). Elements are found in Table 6. Residual vectors are plotted for each observation, two or three at each epoch; see Table 2.

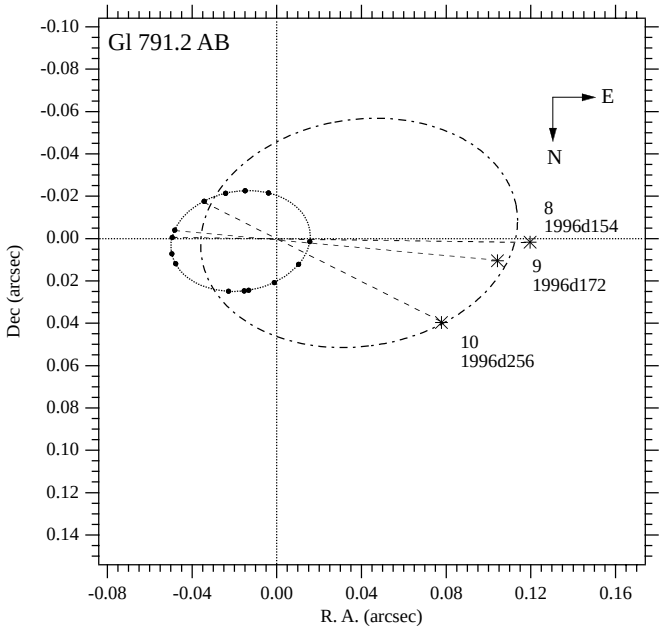

FIG. 4.—Gl 791.2A (*circles*; POS measurements) and Gl 791.2B (*asterisks*; TRANS detections). Component B positions are labeled with their corresponding observation set numbers (Table 3). All observations, both POS and TRANS, were used to derive the orbital elements in Table 6.

average absolute value residual, $\langle |\text{res}| \rangle = 1.0$ mas. The three TRANS mode separations and position angles are plotted with the derived component A and B orbits in Figure 4. We note that the three vectors connecting the two components intersect very near the center of mass.

2.4. *Component Magnitude Difference*

For the three epochs listed in Table 3 we were able to obtain a reliable measure of Δm (more precisely, ΔF583W) for component separations along both the X and Y axes. As discussed in Henry et al. (1999), the ΔF583W value along the X axis is usually smaller than that along the Y axis, presumably because the X-axis transfer function is degraded relative to Y. We have therefore derived a correction using 63 FGS 3 observations of 12 systems (Henry et al. 1999). This correction, amounting to $+0.08$ mag, is far less than the obvious scatter in our measurements. Nonetheless, applying the correction to only the $\Delta F583W_X$, we obtain the Δm_X^c values shown in Table 3. By averaging both axes, we obtain a final $\Delta F583W = 3.32 \pm 0.10$, for which we have adopted the error as described in Henry et al. (1999). Finally, a slight conversion is required from the F583W filter to the V band, as described in the same paper, and we have a final value of $\Delta V = 3.27 \pm 0.10$.

3. Gl 791.2 TOTAL AND COMPONENT MASSES

The orbit (Table 6 and Fig. 4) provides the total separation, a, and α_A, the perturbation orbit size. Because at each instant in the orbits of the two components around the common center of mass,

$$M_A/M_B = \alpha_B/\alpha_A \,, \tag{5}$$

we can express the mass fraction as

$$f = M_B/(M_A + M_B) = \alpha_A/(\alpha_A + \alpha_B) \,, \tag{6}$$

where $\alpha_B = a - \alpha_A$. From the three epochs of component B detection we derive a mass fraction of 0.3051 ± 0.0031. From the orbit parameters in Table 6, $\alpha_A = 33.2 \pm 0.3$ mas.

TABLE 7

GL 791.2 COMPONENT MASSES AND M_V

Parameter	Value
M_{tot}	$0.412 \pm 0.009\ M_\odot$
M_A	$0.286 \pm 0.006\ M_\odot$
M_B	$0.126 \pm 0.003\ M_\odot$
M_A	13.37 ± 0.03
M_B	16.64 ± 0.10

For comparison, the semimajor axis of the photocentric orbit was found to be 29 mas by Harrington (1971) and 28 ± 2 mas by Hershey (1978), although our new value has an error ~ 10 times smaller.

Our measured semimajor axis ($a = 108.8 \pm 0.7$ mas), the period ($P = 1.4731 \pm 0.0008$ yr), and the absolute parallax (112.9 ± 0.3 mas), provide an orbit semimajor axis of 0.963 ± 0.007 AU and a total system mass $M_{tot} = 0.412 \pm 0.009\ M_\odot$, from Kepler's third law. From the mass fraction we derive $M_A = 0.286 \pm 0.006\ M_\odot$ and $M_B = 0.126 \pm 0.003\ M_\odot$, which are masses with only 2% formal error.

4. Gl 791.2 A AND Gl 791.2B ON THE MLR

With the component masses determined, we require the component absolute magnitudes to place these stars on the MLR. We use the photometry of both components from Leggett (1992), $V = 13.06 \pm 0.03$, our measured $\Delta V = 3.27 \pm 0.10$, and our parallax, $\pi_{abs} = 112.9 \pm 0.3$ mas, to derive $M_{VA} = 13.37 \pm 0.03$ and $M_{VB} = 16.64 \pm 0.10$. For this very nearby system we have assumed no absorption ($A_V = 0$). We collect all derived mass and absolute magnitude values in Table 7.

Components A and B lie on the MLR as shown in Figure 5, with Gl 791.2 B one of the lowest mass objects on the lower main sequence. The lower main-sequence relation is from Henry et al. (1999). The straight-line higher mass section ($M > 0.2\ M_\odot$) is from Henry & McCarthy (1993). The distance between the present locus of the MLR and our results for Gl 791.2 requires some comment. First we suggest that Gl 791.2 A and B are underluminous. This is possible if they have metallicity higher than solar. Recent M dwarf models (Baraffe et al. 1998) show that the absolute magnitude of an M dwarf depends not only on mass, but also on age (evolutionary stage) and very sensitively on metallicity. Higher metallicity stars have fainter M_V than lower metallicity stars. This is the explanation offered by Delfosse et al. (1999) for Gl 866 ABC, also subluminous compared with their MLR. The rapid rotation ($V_{rot} = 32$ km s^{-1}) and young disk kinematics of Gl 791.2. Delfosse et al. (1998) support relatively recent formation and hence, probably higher than solar metallicity. Second, because the astrometric residuals for Gl 791.2A (Table 2 and Figure 3) are larger than those we typically obtain, some of the perceived underluminosity might rather be a consequence of excess mass due to an undetected short-period, low-mass companion.

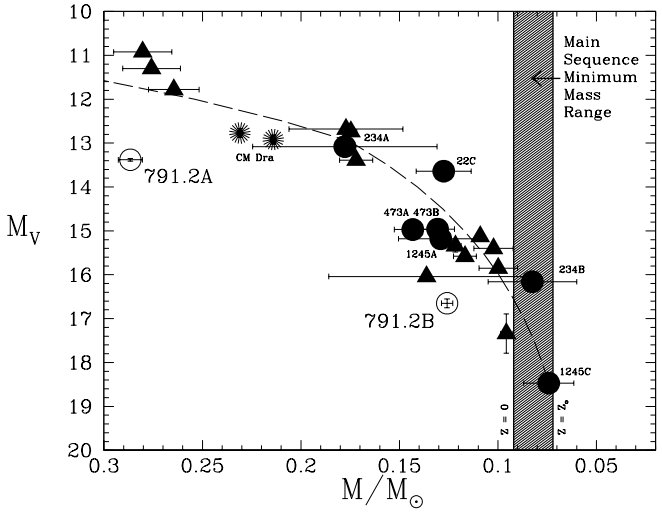

FIG. 5.—Components of Gl 791.2 on the mass-luminosity diagram, showing masses determined by our group (*circles*), orbits and masses determined by others (*triangles*), and the two components of the eclipsing binary CM Draconis (*asterisks*). The curve represents the empirical mass-luminosity relation from Henry & McCarthy (1993) for masses down to $0.18\ M_\odot$ and from Henry et al. (1999) for lower masses. The shaded region with borders at 0.092 and $0.072\ M_\odot$ marks the main-sequence minimum mass range for objects with zero to solar metallicity.

5. CONCLUSIONS

1. Observations of the low-mass binary Gl 791.2 with *HST* FGS 3 over a 1.7 yr time span yield a parallax with an external error better than 1%.

2. Fringe-tracking observations of the primary, component A, provide a well-determined perturbation orbit. In this case a large ΔV produces very small and correctable effects on the interferometer response function, permitting high-precision positional measurements.

3. Demonstrating the difficulty of measuring both components of large ΔV targets with *HST*, fringe-scanning observations succeeded only about 20% of the time, but they provide a mass fraction, 0.3051 ± 0.0031, and $\Delta V = 3.27 \pm 0.10$. The component magnitude difference was obtained only at epochs of largest separation.

4. We obtain masses precise to 2%: $M_{tot} = 0.412 \pm 0.009\ M_\odot$, $M_A = 0.286 \pm 0.006\ M_\odot$ and $M_B = 0.126 \pm 0.003 M_\odot$.

5. These masses and absolute magnitudes assist in defining the lower main-sequence MLR. The dependence of the lower main-sequence MLR on metallicity is an important question for the future.

This research has made use of the NASA Astrophysics Data System Abstract Service and the SIMBAD Stellar Database inquiry and retrieval system. World Wide Web access to the astrometry and photometry in USNO-A2.0 is gratefully acknowledged. Support for this work was provided by NASA through grants GTO NAG5-1603, GO 06036.01-94A, and GO 07491.01-97A from the Space Telescope Science Institute, which is operated by the Association of Universities for Research in Astronomy, Inc., under NASA contract NAS 5-26555. Denise Taylor provided crucial scheduling assistance at the Space Telescope Science Institute. We thank Thierry Forveille for an early copy of the Gl 866 results. An anonymous referee made several suggestions that prompted a revisit to these data, resulting in a better paper.

REFERENCES

Baraffe, I., Chabrier, G., Allard, F., & Hauschildt, P. H. 1998, A&A, 337, 403
Bradley, A., Abramowicz-Reed, L., Story, D., Benedict, G., & Jefferys, W. 1991, PASP, 103, 317
Benedict, G. F., et al. 1999, AJ, 118, 108
———. 1998, Proc. SPIE, 3350, 229
Burrows, A., Hubbard, W. B., Saumon, D., & Lunine, J. I. 1993, ApJ, 406, 158
Delfosse, X., Forveille, T., Perrier, C., & Mayor, M. 1998, A&A, 331, 581
Delfosse, X., Forveille, T., Udry, S., Beuzit, J.-L., Mayor, M., & Perrier, C. 1999, A&A, 350, L39
Franz, O. G., et al. 1998, AJ, 116, 1432
Harrington, R. S. 1971, AJ, 76, 930
Harrington, R. S., & Dahn, C. C. 1980, AJ, 85, 454
Harrison, T. E., McNamara, B. J., Szkody, P., McArthur, B. E., Benedict, G. F., Klemola, A. R., & Gilliland, R. L. 1999, ApJ, 515, L93
Henry, T. J. 1998, ASP Conf. Ser. 134, Brown Dwarfs and Extrasolar Planets, ed. R. Rebolo, E. L. Martin, & M. R. Zapatero Osorio (San Francisco: ASP), 28
Henry, T. J., Franz, O. G., Wasserman, L. H., Benedict, G. F., Shelus, P. J., Ianna, P. A., Kirkpatrick, J. D., & McCarthy, D. W. 1999, ApJ, 512, 864
Henry, T. J., & McCarthy, D. W., Jr. 1993, AJ, 106, 773
Hershey, J. 1978, AJ, 83, 308
Jefferys, W. H., Fitzpatrick, M. J., & McArthur, B. E. 1987, Celest. Mech., 41, 39
Kirkpatrick, J. D., Henry, T. J., & McCarthy, D. 1991, ApJS, 77, 417
Leggett, S. K. 1992, ApJS, 82, 351
McArthur, B. E., et al. 1999, ApJ, 520, L59
McCarthy, D. W., Jr. 1986, in Astrophysics of Brown Dwarfs, ed. M. C. Kafatos, R. S. Harrington, & S. P. Maran (Cambridge: Cambridge Univ. Press), 9
Metcalfe, T. S., Mathieu, R. D., Latham, D. W., & Torres, G. 1996, ApJ, 456, 356
Monet, D. G. 1998, BAAS, 193, 112.003
Standish, E. M. J. 1990, A&A, 233, 252
van Altena, W. F., Lee, J. T., & Hoffleit, E. D. 1995, The Yale Parallax Catalog (4th ed.; New Haven: Yale Univ. Observatory)
van de Kamp, P. 1967, Principles of Astrometry (San Francisco: Freeman)